MDPI

Giant Spin Current Rectification Due to the Interplay of Negative Differential Conductance and a Non-Uniform Magnetic Field

Kang Hao Lee [1], Vinitha Balachandran [1],*, Ryan Tan [2], Chu Guo [3] and Dario Poletti [1,2,*]

[1] Science, Mathematics and Technology Cluster, Singapore University of Technology and Design, 8 Somapah Road, Singapore 487372, Singapore; kanghao_lee@mymail.sutd.edu.sg

[2] Engineering Product Development Pillar, Singapore University of Technology and Design, 8 Somapah Road, Singapore 487372, Singapore; ryanguangting.tan@unibas.ch

[3] Key Laboratory of Low-Dimensional Quantum Structures and Quantum Control of Ministry of Education, Department of Physics and Synergetic Innovation Center for Quantum Effects and Applications, Hunan Normal University, Changsha 410081, China; guochu604b@gmail.com

* Correspondence: vinitha_balachandran@sutd.edu.sg (V.B.); dario_poletti@sutd.edu.sg (D.P.)

check for updates

Abstract: In XXZ chains with large enough interactions, spin transport can be significantly suppressed when the bias of the dissipative driving becomes large enough. This phenomenon of negative differential conductance is caused by the formation of two oppositely polarized ferromagnetic domains at the edges of the chain. Here, we show that this many-body effect, combined with a non-uniform magnetic field, can allow for a high degree of control of the spin current. In particular, by studying all of the possible shapes of local magnetic fields potentials, we find that a configuration in which the magnetic field points up for half of the chain and down for the other half, can result in giant spin-current rectification, for example, up to 10^8 for a system with only 8 spins. Our results show clear indications that the rectification can increase with the system size.

1. Introduction

Quantum spin systems exhibit rich transport properties. For instance, tuning the interactions in the system, spin transport can change from ballistic to diffusive [1–4]. One effect that is particularly relevant for our work is the emergence of negative differential conductance (NDC), which is the phenomenon, whereby the spin current decreases as the bias that is imposed by the spin baths increases [5,6]. Such an apparently counterintuitive phenomenon is due to the fact that the interplay between the dissipative driving and the interactions in the system result in the formation of ferromagnetic domains at the edges of the chain, which significantly suppress the spin current. The effect can be so strong that the spin chain becomes an insulator.

Here, we study a boundary driven XXZ spin chain in the NDC regime in the presence of a non-uniform external magnetic field. In order to obtain more generic conclusions, we consider the magnetic field that locally can only take two possible values $\pm h$. A detailed analysis of the effect of different shapes of the magnetic field potential shows that two configurations, such that the magnetic field is in one direction

in half of the chain and in the other direction for the other half, strongly enhance or even more strongly suppress the ferromagnetic domains. This results, respectively, in the smallest or largest spin currents between all of the possible shapes of the magnetic field potential. Because these two configurations are mirror-symmetric, this implies that, if the field points for half the chain in one direction, and for the other half in the opposite direction, then one can obtain a giant rectification effect, which, we show can be of the order of 10^8 already for small spin chains. The currents and rectification also show a resonant behavior that we correlate to the presence of avoided crossings in the energy spectrum of the bulk Hamiltonian. An analysis of the delocalization of the eigenstates of the Hamiltonian indicates that this giant rectification is also present in the thermodynamic limit.

This work adds to the recent results on rectification in spin chains without local magnetic fields [7,8], with disorder [9] or with external fields [10–15]. Importantly, to the best of our knowledge, in no previous work, strong rectification was connected to the possible emergence of NDC. The manuscript is organized, as follows: in Section 2, we describe our model and, in Section 3, we discuss our results. Last, in Section 4, we draw our conclusions.

2. Model

We consider an XXZ spin chain of length L with the following Hamiltonian

$$\hat{\mathcal{H}} = \sum_{i=1}^{L-1} 2J(\hat{\sigma}_i^+ \hat{\sigma}_{i+1}^- + \hat{\sigma}_i^- \hat{\sigma}_{i+1}^+) + J_{zz}\hat{\sigma}_i^z \hat{\sigma}_{i+1}^z + \sum_{i=1}^{L} h_i \hat{\sigma}_i^z, \tag{1}$$

where $\hat{\sigma}_i^\pm$ are the raising and lowering operators acting on site i and $\hat{\sigma}_i^z$ is a Pauli spin matrix. J and J_{zz} denote the tunneling strength and magnitude of the nearest neighbor interaction, respectively. We use h_i for the local magnetic field. On each site, the local magnetic field h_i can only take the two discrete values $\pm h$. Therefore, there are 2^L possible shapes of magnetic field potential.

The chain is coupled to two spin baths at the edges and we model the evolution via a Gorini–Kossakowski–Sudarshan–Lindblad (GKSL) master equation [16,17] for the system density matrix as [3,12,18–24]

$$\frac{\partial \hat{\rho}}{\partial t} = -\frac{i}{\hbar}[\hat{\mathcal{H}}, \hat{\rho}] + \sum_{j=1}^{4} \hat{\Gamma}_j \hat{\rho} \, \hat{\Gamma}_j^\dagger - \frac{1}{2}\sum_{j=1}^{4}\{\hat{\Gamma}_j^\dagger \hat{\Gamma}_j, \hat{\rho}\}, \tag{2}$$

where the $\hat{\Gamma}_j$ are the jump operators given by

$$\hat{\Gamma}_1 = \sqrt{\gamma\mu_1}\hat{\sigma}_1^+, \qquad\qquad \hat{\Gamma}_2 = \sqrt{\gamma(1-\mu_1)}\hat{\sigma}_1^-, \tag{3}$$

$$\hat{\Gamma}_3 = \sqrt{\gamma\mu_L}\hat{\sigma}_L^+, \qquad\qquad \hat{\Gamma}_4 = \sqrt{\gamma(1-\mu_L)}\hat{\sigma}_L^-. \tag{4}$$

Here, γ describes the system-reservoir coupling strength and μ_1 (μ_L) is the left (right) dissipation bias. We choose a symmetric driving at the boundaries, i.e., $\mu_{1,L} = (1\mp\mu)/2$. Thus, $\mu \equiv \mu_L - \mu_1 \in [-1,1]$ is the dissipative boundary driving bias, due to the reservoirs. In the limiting case with $\mu = 1$, so that $\mu_1 = 0$ and $\mu_L = 1$, the left reservoir tries to impose spin up to spin down conversions, while the right reservoir would do the opposite, only converting spins down to spins up. For the rest of the paper, in the study of our systems, we will be using $\mu = 1$, which is the largest possible bias , and we will refer to this as the strong driving regime.

For $\mu \neq 0$, the system relaxes to a current carrying non-equilibrium steady state (NESS) $\hat{\rho}_{ss}$ at long times. The spin current $\mathcal{J}$ can be obtained from the continuity equation for local magnetisation $\hat{\sigma}_i^z$,

$$\frac{d\hat{\sigma}_i^z}{dt} = \hat{j}_{i-1} - \hat{j}_i,$$

(5)

resulting in $\mathcal{J} = \text{Tr}(\hat{j}_i \hat{\rho}_{ss})$, where $\hat{j}_i = 4iJ(\hat{\sigma}_i^- \hat{\sigma}_{i+1}^+ - \hat{\sigma}_i^+ \hat{\sigma}_{i+1}^-)/\hbar$. In the steady state, the current is independent of the chosen site i. For all systems considered in this study, the steady state density matrix $\hat{\rho}_{ss}$ is computed by setting the time derivative to zero in Equation (2) and using exact diagonalization with a number conserving numerical approach described in [25], which allows for studying open spin systems up to 14 spins. From the point of view of numerical computations, we stress that, to simulate with exact diagonalization the density matrix for L spins, one would require storing a state with 2^{2L} elements, which corresponds to simulating the unitary dynamics of a system with $2L$ spins. This poses a severe limit to the system sizes that one can compute in reasonable time. In the following, we work in units, for which J and $\hbar$ are 1.

3. Results

Interactions in the XXZ chain can significantly alter the spin transport in a boundary driven chain. For instance, in the absence of any field and for $\mu = 1$, the spin current is ballistic for $|J_{zz}/J| < 1$ (weakly interacting), super diffusive for $|J_{zz}/J| = 1$, and insulating for $|J_{zz}/J| > 1$ (strongly interacting). The insulating behavior at large bias results in the interesting phenomenon of negative differential conductance in strongly interacting ($|J_{zz}/J| > 1$) XXZ chains [5,6]. The insulating behavior is attributed to the formation of two oppositely polarized ferromagnetic domains in the chain, each half of the chain acquiring the polarisation of the reservoir to which it is connected. The two domains inhibit the spin flips that result in the reduction of current in the chain. The main focus of this paper is to explore the potential advantages of these ferromagnetic domains in device applications. To this end, we apply a local magnetic field in all of the possible shapes of magnetic field potential configurations, as presented in Equation (1) to the XXZ chain and study the spin transport.

We start by considering, in Figure 1, the spin current $\mathcal{J}$ versus interaction J_{zz} for all of the 2^L configurations of the magnetic field. We highlight that the presence of fewer lines as compared to 2^L in these panels is due to the fact that some different configurations of magnetic fields result in the same current. For instance, there are only 10 plots in Figure 1a, and this is due to the fact that there are six pairs of magnetic field configurations that yield the same $\mathcal{J}$ versus J_{zz} profile within the pair. In the following, we use the following notation in order to indicate the magnetic fields direction: we write a $+$ for a site with magnetic field $+h$ and $-$ for a site with field $-h$. For instance, $(+, -, -, +)$ corresponds to the magnetic field configuration $(+h, -h, -h, +h)$. For the case in which the magnetic field is h in the first half of the chain, and $-h$ in the second half of the chain, we refer to it as $(+, \cdots +, -, \cdots -)$, the magnetic field, which is $-h$ in the first half of the chain and $+h$ in the second half, we refer to it as $(-, \cdots -, +, \cdots +)$. Note that the configuration $(+, \cdots +, -, \cdots -)$ is highlighted by the red dotted line, while its reflection symmetric configuration $(-, \cdots -, +, \cdots +)$ is depicted by the blue dashed line while all the other configurations by represented by grey lines. For J_{zz} large enough we observe that the configurations corresponding to the blue and the red lines are either the ones with the largest or the lowest currents. This is very clearly observed for system sizes $L = 4$ to 8.
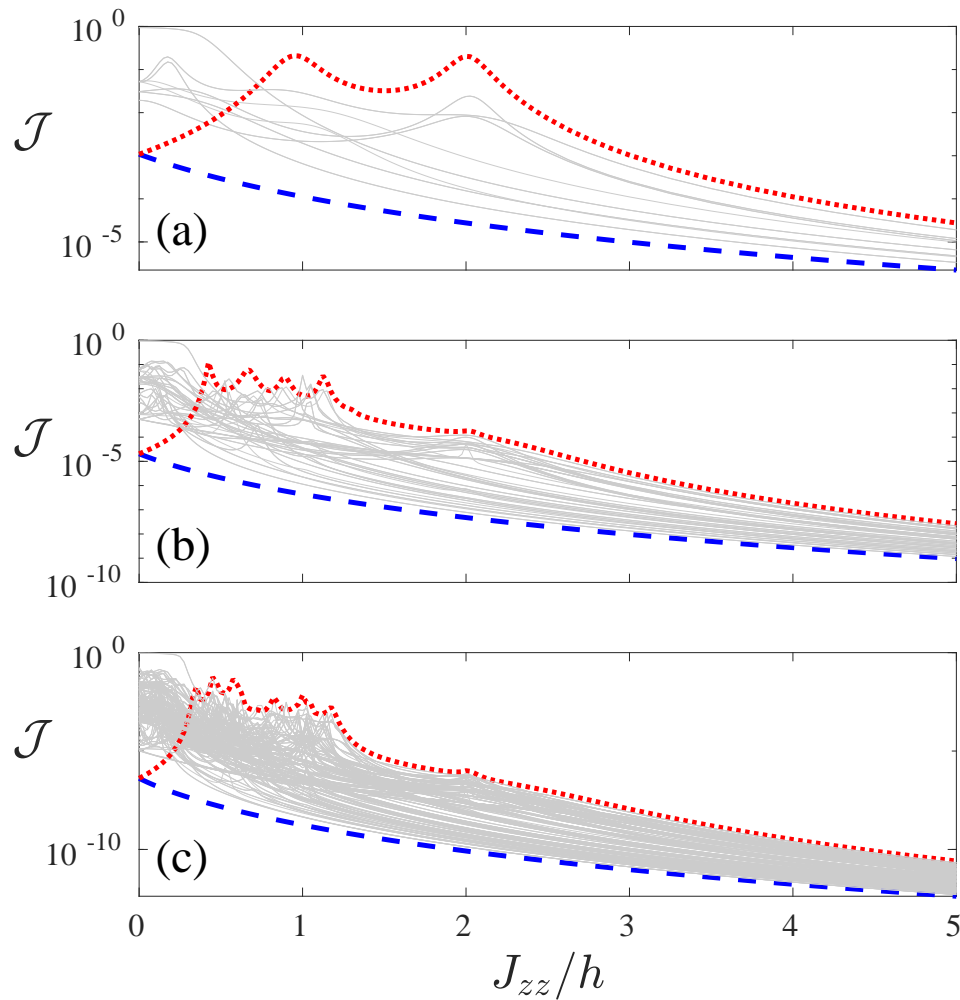
Figure 1. Spin current $\mathcal{J}$ as a function of the ratio of interaction and local field strength J_{zz}/h for system sizes $L = 4$ (**a**), $L = 6$ (**b**) and $L = 8$ (**c**). Different lines corresponds to each of the 2^L magnetic field configurations. We highlight two magnetic field configurations: with the red dotted line, we show the current for a field, which is h for the first half of the chain, and $-h$ for the second half of the chain, which we refer to as $(+, \ldots, +, -, \ldots, -)$, and with the blue dashed line the realization in which the field is $-h$ in the first half of the chain and h in the second half $(-, \ldots, -, +, \ldots, +)$. The common parameters are $h = 4$, $\gamma = 1$ and $\mu = 1$.

In Figure 1, we consider a large local field $h = 4$. However, it is insightful to fix the interaction to be large, e.g., $J_{zz} = 4$ and study the current as we vary h. This is depicted in Figure 2. The configuration $(-, -, +, +)$ corresponds (blue dashed line) to the lowest current, while the configuration $(+, +, -, -)$ corresponds, for smaller h, to the largest currents. It also presents some resonant-like structures, and its current decreases for larger values of h. Given this seemingly antithetic effect of the $(-, -, +, +)$ and $(+, +, -, -)$ configurations, which are reflection symmetric of each other, in the following we study the effectiveness of all the different magnetic field configurations in order to result in a large spin current rectification effect.
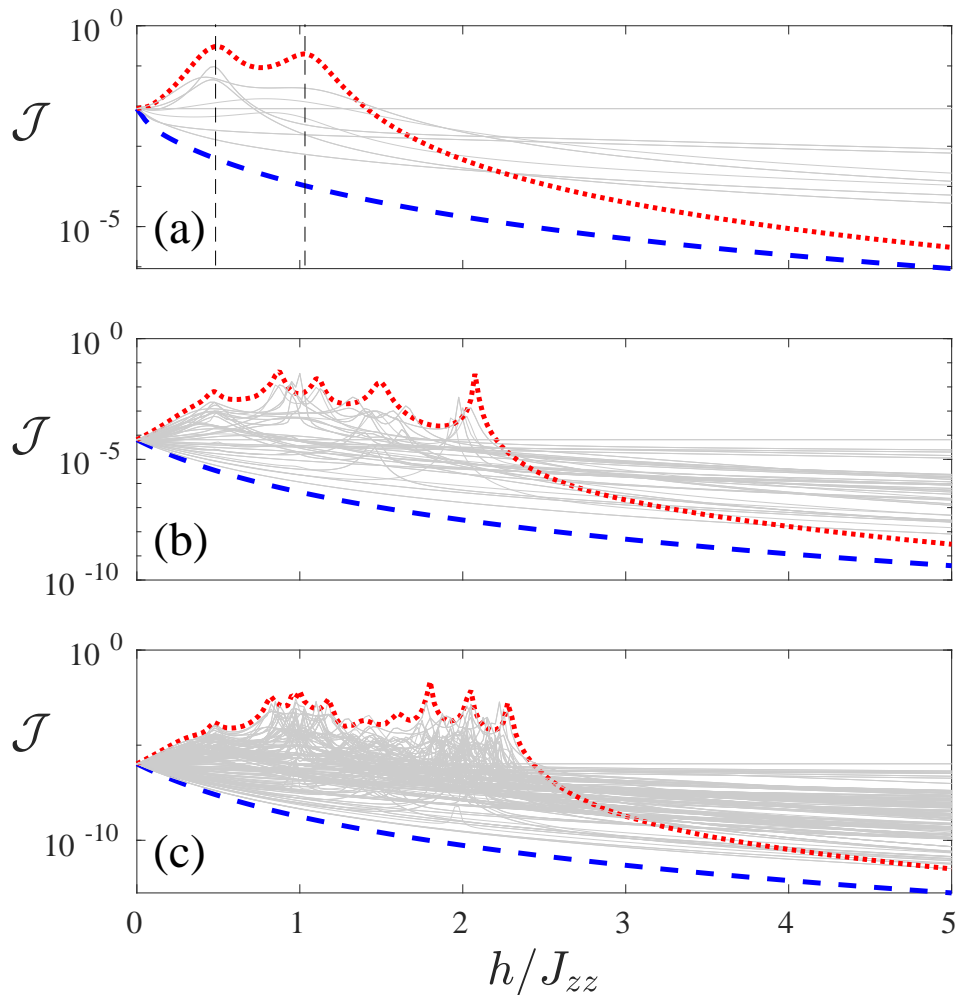
Figure 2. Spin current $\mathcal{J}$ as a function of the ratio of local field strength and interaction h/J_{zz} for system sizes $L = 4$ (**a**), $L = 6$ (**b**) and $L = 8$ (**c**). Different lines corresponds to each of the 2^L configurations of local fields. We highlight two magnetic field configurations: with the red dotted line we show the current for a field, which is h for the first half of the chain, and $-h$ for the second half of the chain, which we refer to as $(+, \ldots, +, -, \ldots, -)$, and with the blue dashed line the realization in which the field is $-h$ in the first half of the chain and h in the second half $(-, \ldots, -, +, \ldots, +)$. Peaks of red dotted line in panel (**a**) are signalled by black dashed lines that correspond to the black dashed lines in Figure 5. Common parameters are $J_{zz} = 4$, $\gamma = 1$ and $\mu = 1$.

Thus, we investigate the rectification in Figure 3. Here, the rectification is quantified using $\mathcal{R} = \mathcal{J}_f / \mathcal{J}_r$ [7,26–28], where $\mathcal{J}_f$ and $\mathcal{J}_r$ are referred to as forward and reverse currents and are computed, respectively, for a configuration of the magnetic field and its reflection symmetric one, e.g., $(+, -, +, -)$ and $(-, +, -, +)$. We note that this is equivalent to fixing a configuration and switching the driving bias (i.e., $\mu = 1$, forward direction to $\mu = -1$, reverse direction). When $\mathcal{R} = 1$, there is no rectification as the forward and reverse currents are equal, e.g., for symmetric magnetic fields configurations. Perfect diodes are signalled by $\mathcal{R} = \infty$ or 0 (the latter is obtained when the forward current tends to 0, but the reverse current is finite). In Figure 3, there are less lines when compared to Figures 1 and 2, and this is due to the fact that each line corresponds to a pair of magnetic field configurations: one is a configuration and the other is the reflection symmetric one. Importantly, each pair is considered only once, e.g., we plot the

rectification considering the $(+, -, +, -)$ configuration to give the forward current $\mathcal{J}_f$ and $(-, +, -, +)$ to give the reverse current $\mathcal{J}_r$, and we do not plot the opposite combination, because it does not give extra information, resulting in a $1/\mathcal{R}$ rectification. This is particularly relevant, because, in Figure 3, we use a log-lin plot, and the reverse combination of magnetic field configurations would simply result in a curve symmetric around $\mathcal{R} = 1$. The blue thick line presented in Figure 3 corresponds to the combination $(+, \ldots, +, -, \ldots, -)$, for $\mathcal{J}_f$, and $(-, \ldots, -, +, \ldots, +)$, for $\mathcal{J}_r$, and it gives clearly the strongest rectification. We remind the reader that a small value of $\mathcal{R}$ corresponds to a large rectification in the opposite direction, yet clearly the blue thick line corresponds to the largest possible current rectifications. In Figure 3, we also note that, for larger systems, one can obtain even larger rectifications, for example, showing a rectification of $\mathcal{R} \approx 10^8$ for the $L = 8$ chain. We will also return to this point in a later part of the paper.
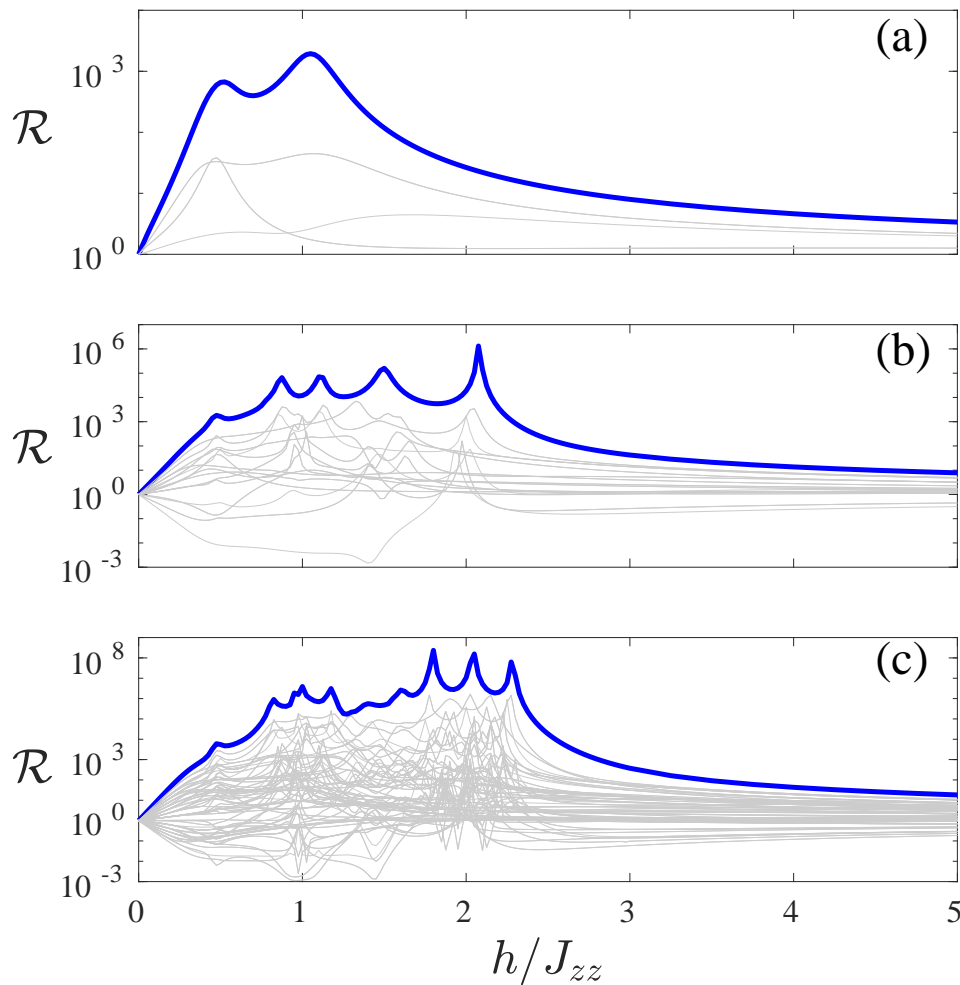
Figure 3. Rectification $\mathcal{R}$ is plotted as a function of the ratio of local field strength and interaction h/J_{zz} for system sizes $L = 4$ (**a**), $L = 6$ (**b**) and $L = 8$ (**c**). The current $\mathcal{J}_f$ with magnetic field configuration as $(+, \ldots, +, -, \ldots, -)$ and $\mathcal{J}_r$ for $(-, \ldots, -, +, \ldots, +)$ are highlighted as thick blue lines. The other configurations are in thin grey lines. Common parameters are $J_{zz} = 4$, $\gamma = 1$, $\mu = 1$.

In Figure 4, rectification $\mathcal{R}$ is plotted as a function of interaction J_{zz}. Similar to Figure 3, each line corresponds to a pair of magnetic field configurations, which are the reflection symmetric of each other. Highlighted in blue thick line is the $(+, \cdots +, -, \cdots -)$, $(-, \ldots, -, +, \ldots, +)$ configuration pair which

yields the strongest rectification. Here, we highlight the role of interaction J_{zz} in causing large rectification. In panel (a) of Figure 4, where $h = 0.1$, we observe the sharp transition to a steep increase in rectification occuring near $J_{zz} = 1$, where the quantum phase transition occurs. This transition occurs at smaller values of J_{zz} for increasing h, as we observe for $h = 1$ in panel (b) and $h = 3$ in panel (c). With increasing h, the system behaviour deviates further from that of the XXZ spin chain system, and it is thus natural that the values of J_{zz}, for which an enhancement of rectification occur, deviates further from $J_{zz} = 1$. Figure 4 thus highlights the importance of the interplay of kinetic, interactive, and dissipative terms in the master Equation (2) of the set-up.
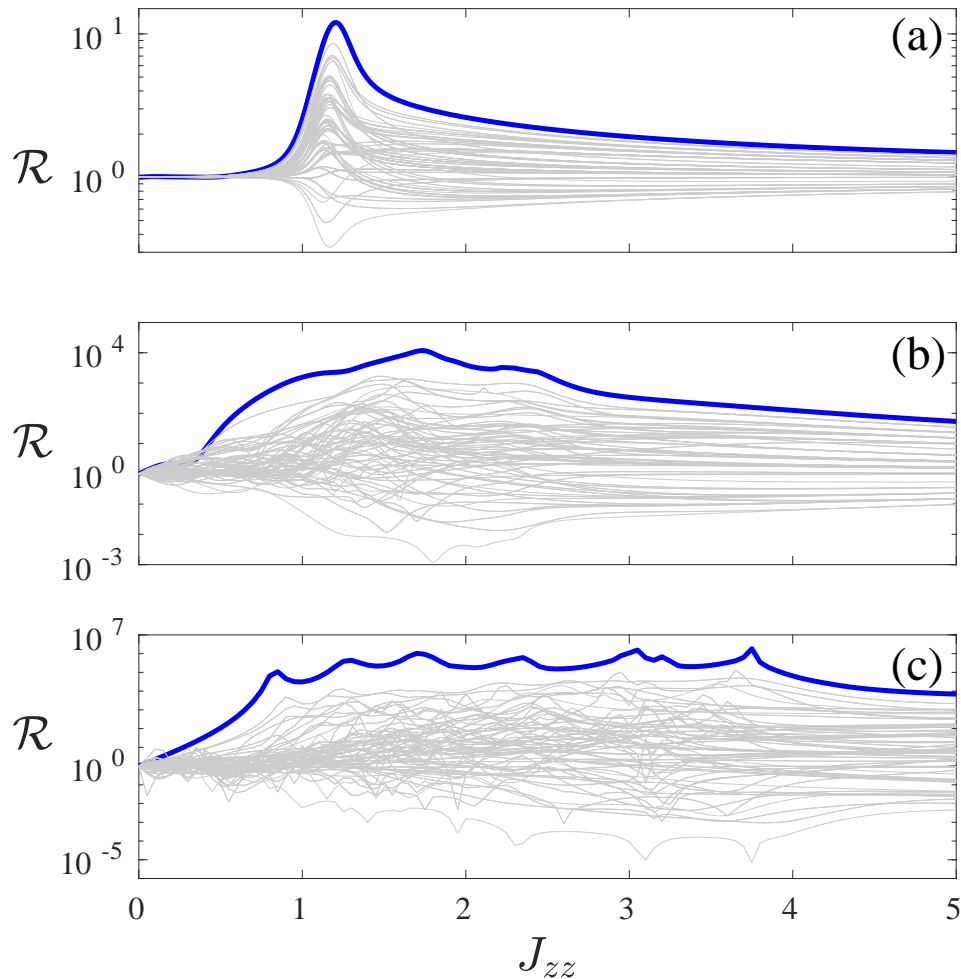
Figure 4. Rectification $\mathcal{R}$ is plotted as a function of interaction J_{zz} for $h = 0.1$ (**a**), $h = 1$ (**b**) and $h = 3$ (**c**) for a system size of $L = 8$. The rectification as ratio of current $\mathcal{J}_f$ with magnetic field configuration as $(+, \ldots, +, -, \ldots, -)$ and $\mathcal{J}_r$ for $(-, \ldots, -, +, \ldots, +)$ are highlighted as thick blue lines. The other configurations are in thin grey lines. The common parameters are $\gamma = 1$, $\mu = 1$.

In Figures 1–4, we have observed resonances, which correspond to peaks of currents and the largest rectifications. We now aim to gain an insight into this. The mechanism for the emergence of such resonances, and of the strong rectifications, can be understood by studying the configuration $(+, \cdots +, -, \cdots -)$, where the field is in the positive direction in first half of the chain and negative in the other half of the chain (the configuration corresponding to the largest rectification). To give a clear idea of

the mechanism, we focus on the case of $L = 4$. In Figure 5, we show the energy spectrum as a function of h for $J_{zz} = 4$. For each magnitude h, the value of the energy is indicated by a point in the plot. Different colors of each point corresponds to the values of the overlap of the corresponding eigenvector $|\psi_s\rangle$ with the state $|\downarrow\downarrow\uparrow\uparrow\rangle$, i.e., $|\langle\psi_s|\downarrow\downarrow\uparrow\uparrow\rangle|^2$. The vertical dashed lines show the position of the peaks of current for system size $L = 4$, as taken from Figure 2. It is clear from the figure that the avoided crossings in the spectrum matches with the maxima of the current. At these points, given the proximity in energy between different energy eigenstates, it is easier for the steady state to be in a mixture of different eigenstates, thus resulting in the possibility of larger currents (note that each energy eigenstate carries 0 current). The presence of avoided crossings for the peaks in Figures 1–3 has been checked for all system sizes and parameters tested.
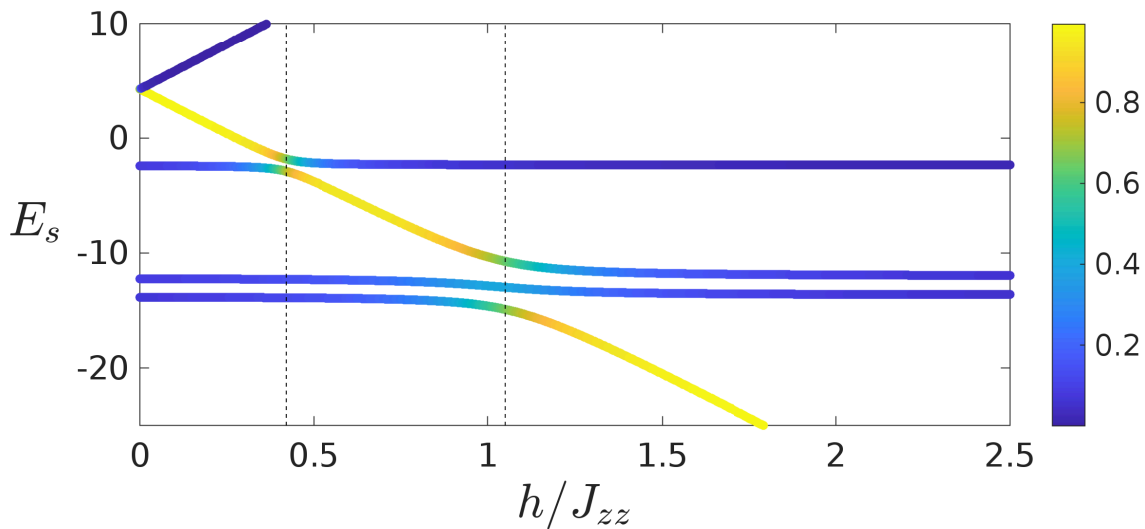
Figure 5. Eigenenergies E_s in the zero magnetisation sector of a chain of length $L = 4$ with magnetic field configuration $(+, +, -, -)$ plotted as a function of the ratio of local field strength and interaction h/J_{zz}. The vertical lines in each panel correspond to peaks in the current as from Figure 2a. The color that is used for the eigenenergies corresponds to the overlap between the eigenvector and the state $|\downarrow\downarrow\uparrow\uparrow\rangle$. Parameters: $\gamma = 1, \mu = 1, J_{zz} = 4$.

Thus, we have shown that an XXZ chain with large enough interaction J_{zz} and a magnetic field in the configuration $(+, \cdots+, -, \cdots-)$ results in a highly performing spin-current diode. It is however important to investigate the performance at larger sizes of this diode. At this point we should stress that computing the steady state in regimes of very low currents is extremely demanding, because the equations are ill-conditioned. Thus, we resort to a different, yet very insightful approach. In order to understand the robustness of the effect for larger system sizes, we study the inverse participation ratio (IPR) of the Hamiltonian of the system with the local magnetic field configuration $(+, \dots, +, -, \dots, -)$ in Figure 6. The IPR for a given state $|\psi\rangle$ over the energy eigenstates $|n\rangle$ is given by $IPR = \sum_n |\langle n|\psi\rangle|^4$. A value of $1 - IPR \approx 1$ means that the state $|\psi\rangle$ is well distributed over all the eigenstates $|n\rangle$, while $1 - IPR \approx 0$ means that $|\psi\rangle$ almost exactly corresponds to a single energy eigenstate. The study of this quantity can be done simply by diagonalizing the Hamiltonian, which we do for system sizes up to $L = 16$.
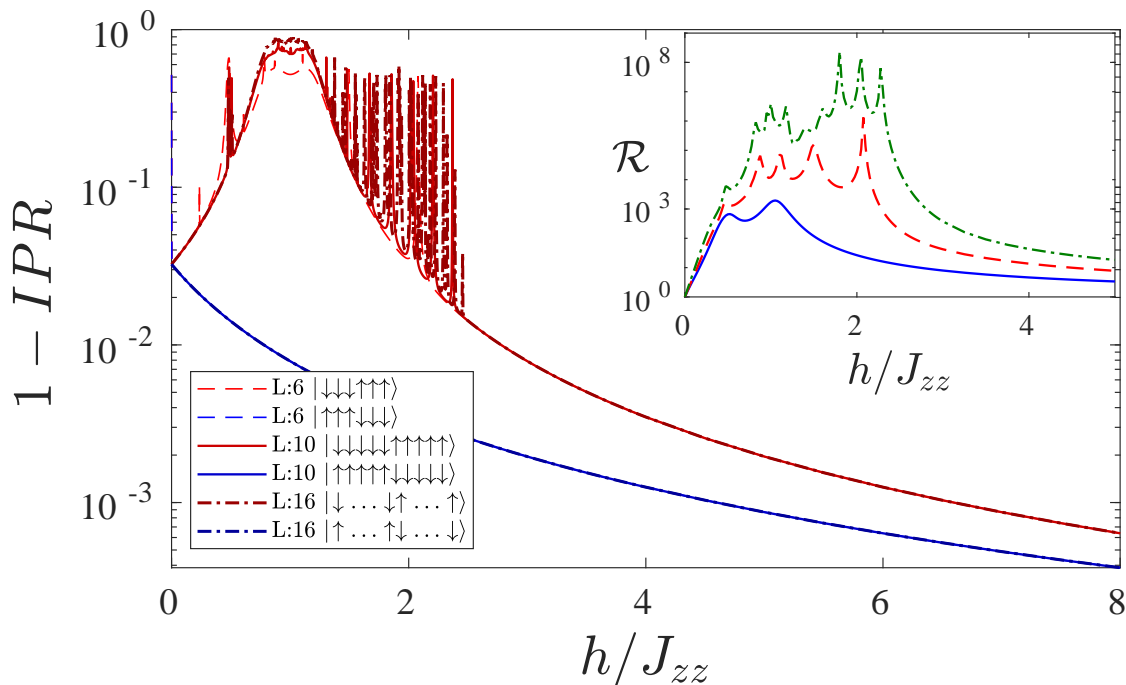
Figure 6. The inverse participation ratio $1 - IPR$ as a function of the ratio of local field strength and interaction h/J_{zz} for different system sizes $L = 16$ (dashed line), $L = 10$ (continuous line) and $L = 6$ (dot-dashed line). Here the magnetic field is in the configuration $(+, \ldots, +, -, \ldots, -)$. Both state configurations $|DU\rangle = |\downarrow \ldots \downarrow \uparrow \ldots \uparrow\rangle$ (red) and $|UD\rangle = |\uparrow \ldots \uparrow \downarrow \ldots \downarrow\rangle$ (blue) are shown. The inset shows the rectification as a function of h/J_{zz} for different system sizes: blue continuous line for $L = 4$, red dashed line for $L = 6$, and green dot-dashed line for $L = 8$. Other parameters are $J_{zz} = 4$, $\gamma = 1$, $\mu = 1$.

In Figure 6, we plot $1 - IPR$ as a function of the ratio of local field strength and interaction h/J_{zz} for the state $|DU\rangle = |\downarrow \ldots \downarrow \uparrow \ldots \uparrow\rangle$ (red plots) and for the state $|UD\rangle = |\uparrow \ldots \uparrow \downarrow \ldots \downarrow\rangle$ (blue plots). For the state $|UD\rangle$, $1 - IPR$ quickly becomes small and it continues to decrease as h increases. This means that the state that is favored by the dissipator in reverse bias, $|UD\rangle$, is almost entirely an eigenstate of the Hamiltonian. Hence, the steady state would be well approximated by this $0-$current-carrying state. We note that the blue solid, dashed, and dot-dashed curves relative to this state, each for a different system size, are almost completely identical.

For the state $|DU\rangle$, the physics is very different. For $h = 0$ $|DU\rangle$ well approximates the highest energetic state, together with $|UD\rangle$. However, while $|UD\rangle$ approximates better and better the highest energetic state as h increases, for large enough magnetic field h, the state $|DU\rangle$ well approximates the ground state. Hence, this state is bound to go through numerous avoided crossings, at the occurrence of which transport is favored and rectification can be very large. In particular, we observe that, for the state $|DU\rangle$, $1 - IPR$ is close to 1 for $h \approx J_{zz}$, and $1 - IPR$ increases with the system sizes. This is because of the presence of a energy band of state that are crossed for $h \approx J_{zz}$. Beyond this energy band, there can be other avoided crossings which can result in even larger rectification. For instance, in the inset of Figure 6, we illustrate the rectification for different system sizes, showing a significant increase in the rectification power as the system size increases, even up to $\mathcal{R} = 10^8$ ($L = 4$ blue continuous line, $L = 6$ red dashed line, and $L = 8$ green dot-dashed line). The exact position of the last avoided crossings depends on the parameters of the system. For large enough J_{zz}/J, they occur for $h \approx 2J_{zz}$. This can be computed analytically, in fact, setting $J = 0$ one realizes that the energy of state $|DU\rangle$ is, for large enough

system sizes L, given by $(L-3)J_{zz} - Lh$ while the energy of the first excited state (at large enough h), is $(L-11)J_{zz} - (L-4)h$. These two energies coincide for $h = 2J_{zz}$. For finite values of J and smaller ratios J_{zz}/J, the last resonance is moved to larger values of h, as in the cases analyzed in this work.

In Figure 7, we plot the steady state Von Neumann entropy $\mathcal{S} = -\mathrm{Tr}(\hat{\rho}_{ss} ln\hat{\rho}_{ss})$. In the reverse bias case (lines with ○), the entropy decreases rapidly as h increases, because the steady state approaches more closely a pure state. This mirrors the results presented in Figure 6, where $|UD\rangle$ in the reverse bias is favoured by the dissipator and is almost entirely an eigenstate of the Hamiltonian. In the case with magnetic field configuration $(+,\ldots,+,-,\ldots,-)$ (lines without symbols), the steady state is mixed and has much larger entropy, particularly at the avoided crossing where the current and the rectification are largest. For even larger magnitude of the magnetic field h, the steady state also approximates a pure state and the entropy decreases.
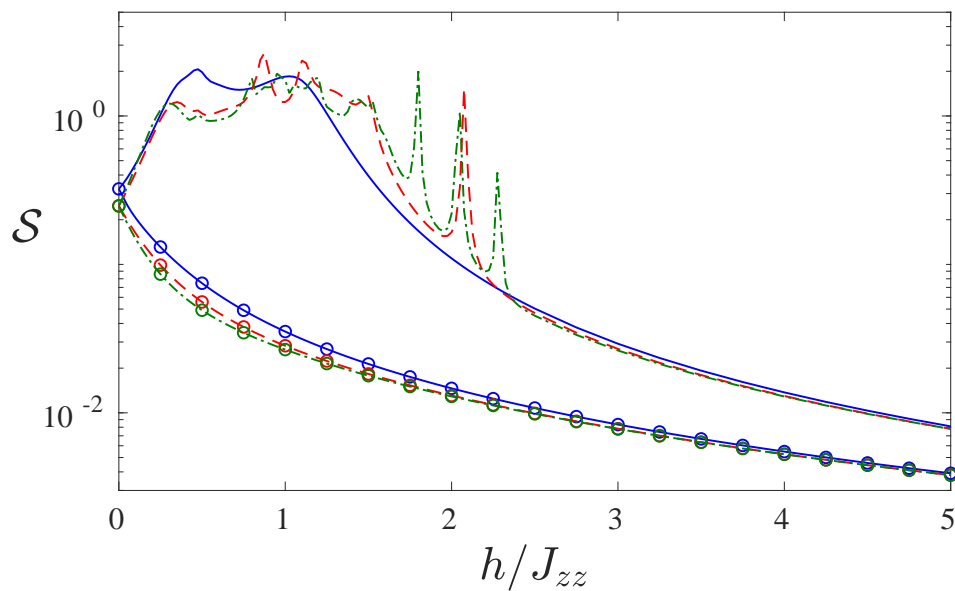
Figure 7. The Von Neumann entropy $\mathcal{S}$ as a function of the ratio of local field strength and interaction h/J_{zz} for system sizes $L = 4$ (blue solid line), $L = 6$ (red dashed line) and $L = 8$ (green dot-dashed line). We show both the entropy of the steady state density matrix ρ_{ss} for the magnetic field configuration $(+,\ldots,+,-,\ldots,-)$ (no symbols) and $(-,\ldots,-,+,\ldots,+)$ (lines with ○). The common parameters are $J_{zz} = 4$, $\gamma = 1$ and $\mu = 1$.

4. Conclusions

We have studied the effect of local magnetic fields on the spin transport of a strongly interacting XXZ chain. We have shown that a configuration with the field pointing in one direction for half the chain and in the opposite direction for the other half can result in giant rectification. This is due to the fact that, in one direction, the magnetic field cooperates with interactions in producing two large ferromagnetic domains, while, in the other direction, the magnetic field opposes such a formation and favors transport. Rectification is particularly enhanced at the occurrence of avoided crossings in the energy spectra of the XXZ chain with this configuration of magnetic field. As an example of giant rectification, for $L = 8$ we find rectifications of the orders of 10^8. We also show that the rectification is not only robust upon increasing the chain length, but strengthened. Moreover, the presence of resonant peaks of rectification can turn this setup into a switch or sensor, being activated by small changes in the magnetic field.

In future works, we could consider the stability of this effect against other forms of dissipation. For instance, dephasing has been shown to suppress negative differential conductance [18], or perturbations, such as long range interactions, have a detrimental effect on negative differential conductance [29]. Another possible direction would be to consider the performance of this diode for heat current rectification [26–28]. More studies could also be done in understanding the role of spatially varying interactions [30].

Abbreviations

The following abbreviations are used in this manuscript:

NDC   Negative Differential Conductivity
GKSL   Gorini-Kossakowski-Sudarshan-Lindblad
NESS   Non-equilibrium steady state

References

1. Prosen, T. Open XXZ Spin Chain: Nonequilibrium Steady State and a Strict Bound on Ballistic Transport. *Phys. Rev. Lett.* **2011**, *106*, 217206. [CrossRef] [PubMed]
2. Žnidarič, M. Spin Transport in a One-Dimensional Anisotropic Heisenberg Model. *Phys. Rev. Lett.* **2011**, *106*, 220601. [CrossRef] [PubMed]
3. Prosen, T. Exact Nonequilibrium Steady State of a Strongly Driven Open XXZ Chain. *Phys. Rev. Lett.* **2011**, *107*, 137201. [CrossRef] [PubMed]
4. Bertini, B.; Heidrich-Meisner, F.; Karrasch, C.; Prosen, T.; Steinigeweg, R.; Žnidarič, M. Finite-temperature transport in one-dimensional quantum lattice models. *arXiv* **2020**, arXiv:2003.03334.
5. Benenti, G.; Casati, G.; Prosen, T.; Rossini, D.; Žnidarič, M. Charge and spin transport in strongly correlated one-dimensional quantum systems driven far from equilibrium. *Phys. Rev. B* **2009**, *80*, 035110. [CrossRef]
6. Benenti, G.; Casati, G.; Prosen, T.; Rossini, D. Negative differential conductivity in far-from-equilibrium quantum spin chains. *EPL* **2009**, *85*, 37001. [CrossRef]
7. Balachandran, V.; Benenti, G.; Pereira, E.; Casati, G.; Poletti, D. Perfect Diode in Quantum Spin Chains. *Phys. Rev. Lett.* **2018**, *120*, 200603. [CrossRef]
8. Balachandran, V.; Benenti, G.; Pereira, E.; Casati, G.; Poletti, D. Heat current rectification in segmented *XXZ* chains. *Phys. Rev. E* **2019**, *99*, 032136. [CrossRef]
9. Balachandran, V.; Clark, S.R.; Goold, J.; Poletti, D. Energy Current Rectification and Mobility Edges. *Phys. Rev. Lett.* **2019**, *123*, 020603. [CrossRef]
10. Arrachea, L.; Lozano, G.S.; Aligia, A.A. Thermal transport in one-dimensional spin heterostructures. *Phys. Rev. B* **2009**, *80*, 014425. [CrossRef]
11. Schuab, L.; Pereira, E.; Landi, G.T. Energy rectification in quantum graded spin chains: Analysis of the *XXZ* model. *Phys. Rev. E* **2016**, *94*, 042122. [CrossRef] [PubMed]
12. Landi, G.T.; Karevski, D. Open Heisenberg chain under boundary fields: A magnonic logic gate. *Phys. Rev. B* **2015**, *91*, 174422. [CrossRef]

13. Pereira, E. Perfect thermal rectification in a many-body quantum Ising model. *Phys. Rev. E* **2019**, *99*, 032116. [CrossRef] [PubMed]

14. Pereira, E. Thermal rectification in classical and quantum systems: Searching for efficient thermal diodes. *EPL* **2019**, *126*, 14001. [CrossRef]

15. Oliveira, D.; Pereira, E.; Lemos, H.C.F. Transport in boundary-driven quantum spin systems: One-way street for the energy current. *J. Phys. A Math. Theor.* **2020**, *53*, 375007. [CrossRef]

16. Gorini, V.; Kossakowski, A.; Sudarshan, E.C.G. Completely positive dynamical semigroups of N-level systems. *J. Math. Phys.* **1976**, *17*, 821–825. [CrossRef]

17. Lindblad, G. On the generators of quantum dynamical semigroups. *Commun. Math. Phys.* **1976**, *48*, 119–130. [CrossRef]

18. Mendoza-Arenas, J.J.; Grujic, T.; Jaksch, D.; Clark, S.R. Dephasing enhanced transport in nonequilibrium strongly correlated quantum systems. *Phys. Rev. B* **2013**, *87*, 235130. [CrossRef]

19. Mendoza-Arenas, J.J.; Al-Assam, S.; Clark, S.R.; Jaksch, D. Heat transport in the *XXZ* Spin Chain. Ballist. Diffus. Regimes Dephasing Enhanc. *J. Stat. Mech. Theory Exp.* **2013**, *2013*, P07007. [CrossRef]

20. Žnidarič, M. Exact solution for a diffusive nonequilibrium steady state of an open quantum chain. *J. Stat. Mech. Theory Exp.* **2010**, *2010*, L05002. [CrossRef]

21. Žnidarič, M.; Horvat, M. Transport in a disordered tight-binding chain with dephasing. *Eur. Phys. J. B* **2013**, *86*, 67. [CrossRef]

22. Karevski, D.; Popkov, V.; Schütz, G.M. Exact Matrix Product Solution for the Boundary-Driven Lindblad *XXZ* Chain. *Phys. Rev. Lett.* **2013**, *110*, 047201. [CrossRef] [PubMed]

23. Prosen, T.; Žnidarič, M. Matrix product simulations of non-equilibrium steady states of quantum spin chains. *J. Stat. Mech. Theory Exp.* **2009**, *2009*, P02035. [CrossRef]

24. Žnidarič, M. Dephasing-induced diffusive transport in the anisotropic Heisenberg model. *New J. Phys.* **2010**, *12*, 043001, [CrossRef]

25. Guo, C.; Poletti, D. Dissipatively driven hardcore bosons steered by a gauge field. *Phys. Rev. B* **2017**, *96*, 165409. [CrossRef]

26. Terraneo, M.; Peyrard, M.; Casati, G. Controlling the Energy Flow in Nonlinear Lattices: A Model for a Thermal Rectifier. *Phys. Rev. Lett.* **2002**, *88*, 094302. [CrossRef]

27. Li, B.; Wang, L.; Casati, G. Thermal Diode: Rectification of Heat Flux. *Phys. Rev. Lett.* **2004**, *93*, 184301. [CrossRef]

28. Li, N.; Ren, J.; Wang, L.; Zhang, G.; Hänggi, P.; Li, B. Colloquium: Phononics: Manipulating heat flow with electronic analogs and beyond. *Rev. Mod. Phys.* **2012**, *84*, 1045–1066. [CrossRef]

29. Droenner, L.; Carmele, A. Boundary-driven Heisenberg chain in the long-range interacting regime: Robustness against far-from-equilibrium effects. *Phys. Rev. B* **2017**, *96*, 184421. [CrossRef]

30. Gu, J.; Liu, S.; Yazback, M.; Cheng, H.P.; Zhang, X.G. Many-body localization from random magnetic anisotropy. *Phys. Rev. Res.* **2019**, *1*, 033183. [CrossRef]